Evaluation of Forced Reflooding Experiments in APWR-Geometry (NEPTUN-III Facility) using the Advanced Computer Code FLUT-FDWR

M. Cigarini
Institut für Neutronenphysik und Reaktortechnik
Projektgruppe LWR-Sicherheit

Kernforschungszentrum Karlsruhe

KERNFORSCHUNGSZENTRUM KARLSRUHE

Institut für Neutronenphysik und Reaktortechnik

Projektgruppe LWR-Sicherheit

KfK 4585

Evaluation of Forced Reflooding Experiments

in APWR-Geometry (NEPTUN-III Facility)

using the Advanced Computer Code FLUT-FDWR

M. Cigarini

Kernforschungszentrum Karlsruhe GmbH, Karlsruhe

Abstract

CIGARINI, Marco :

Evaluation of Forced Reflooding Experiments in APWR-Geometry (NEPTUN-III Facility) using the Advanced Computer Code FLUT-FDWR

A new version of the GRS computer code FLUT, named FLUT-FDWR, was recently developed in KfK in order to provide an adequate computational means for analysing the behaviour of the most important APWR designs during the reflooding phase after a LOCA. The Code was checked by means of post-test calculations of experiments in PWR as well as in a very tight APWR geometry. The present work shows the results of calculations for a wider APWR geometry (NEPTUN-III Facility) and can be seen as a further step in the code validation for APWR applications.

Zusammenfassung

CIGARINI, Marco :

Auswertung von Zwangsflutungsexperimente in FDWR-Geometrie (NEPTUN-III Anlage) durch das fortgeschrittene Rechenprogramm FLUT-FDWR

Eine neue Version des GRS-Rechenprogrammes FLUT, genannt FLUT-FDWR, wurde neuerdings in KfK entwickelt, um eine geeignete Rechenmethode zur Analyse der Flutphase nach einem Kühlmittelverluststörfall bei den wichtigsten FDWR-Entwürfen verfügbar zu machen. Das Programm wurde durch die Nachrechnung von Experimenten in DWR- und in einer sehr engen FDWR-Geometrie überprüft. Die vorliegende Arbeit zeigt die Ergebnisse von Rechnungen, die für eine weitere FDWR-Geometrie (NEPTUN-III Anlage) durchgeführt wurden, und stellt einen weiteren Schritt der Validierung des Programms für FDWR-Anwendungen dar.

Table of Contents

List of Tables

List of Illustrations

Nomenclature

d	fuel rod outer diameter (m)
d_h	hydraulic diameter (m)
d_1	average diameter of the water droplets in the zone of length L immediately downstream of the quench front (m)
d_2	average diameter of the water droplets in the remaining part, beyond the zone of length L, of the dispersed flow region (m)
L	axial length of the zone of dispersed flow film boiling immediately downstream of the quench front where the average droplet diameter d_1 is used (m)
L_0	length L for the reference experiment FLECHT 32114 (m)
p	pressure (Pa); pitch (m)
Q	volumetric power density in the fluid at reflooding beginning (W/m^3)
Q_0	value of Q for the reference experiment FLECHT 32114 (W/m^3)
Q_{rod}	power per fuel rod (W)
R_l, R_v	geometrical parameters for the calculation of the interfacial drag coefficient between vapor and liquid water (m)
t_{q4}	time at which the measure-level 4 is quenched (s)
T_{cl}	cladding temperature at the middle plane at beginning of reflooding (°C)
T_{max}	maximum cladding temperature during reflooding (°C)
v_{fl}	flooding rate (m/s)

Greek

α	void fraction
ΔT	cladding superheat at the beginning of the reflooding phase (°C)
ΔT_0	value of ΔT for the reference experiment FLECHT 32114 (°C)

1. Introduction

In the concept of the Advanced Pressurized Water Reactor (APWR) with inproved uranium utilisation, the main new feature is the introduction of a tight lattice core in order to achieve a higher conversion ratio than in the conventional PWR. For the determination of the optimum design in consideration of the safety requirements it is necessary to establish flexibly-applicable and highly-accurate predictive methods for core thermal-hydraulic behaviour under accident conditions.
For the past few years much work is being made in this field at the Institut für Neutronenphysik und Reaktortechnik of the Kernforschungszentrum-Karlsruhe. The computer codes RELAP5/MOD1-EUR /1/ and FLUT (GRS-Garching) /2/ have been implemented and further improved in this center. New correlations and physical models based on both theoretical and experimental work on thermohydraulics in hexagonal rod bundels with tight lattice have been introduced in the codes and the new developed versions RELAP5-APWR /3/ and FLUT-FDWR[1] /4/ /5/ have been used to analyse the behaviour of three main reference designs of APWR during an Anticipated Transient Without SCRAM (ATWS) and during a Loss of Coolant Accident (LOCA).

The Code FLUT-FDWR, used for the analysis of the reflooding phase of the LOCA, was verified by means of many post-test calculations of forced reflooding experiments in PWR-geometry as well as in a very tight APWR-geometry (FLORESTAN experiment /6/).

In this work the validation of the code is extended to the post-test calculation of 7 tests performed in a wider APWR lattice in the NEPTUN facility. A complete comparison of the results of the calculations with the experiment was not possible as only partial data have been published till now /7//8/.

A pretest calculation for a further NEPTUN-test, which was characterized by a very low flooding rate /9/, was also performed.

---

[1] FDWR = Fortgeschrittener Druckwasserreaktor = Advanced Pressurized Water Reactor.

2. The Computer Code FLUT-FDWR

A few years ago the version No. 5 of the computer code FLUT, developed by the GRS-Garching /2/ for the calculation of the reflooding phase after a LOCA in a PWR-plant of German design, was implemented on the IBM 3090/SIEMENS 7890 computer configuration of the Kernforschungszentrum Karlsruhe.

The hydrodynamic model in FLUT is a two-fluid model with six conservation equations for mass, momentum and energy. The interaction between the phases is modelled by a very simple set of constitutive equations for mass transfer rate, interfacial drag and interfacial heat transfer, which fulfil basic requirements as symmetry of phases, increase of phase interaction with growing deviation from equilibrium and correct behaviour of the disappearing phase (interaction terms gradually decrease as one phase is disappearing), while the dependence on the flow regime appears only indirectly /10/. This proved to be an advantage for the calculations in APWR-Geometry. As a matter of fact most of the presently used flow maps are based on experimental evidences for pipes or for bundles in normal PWR geometry. Their previsions in case of a different geometry may fail completely. The pretest calculations of the first forced reflooding experiment in a very tight APWR Geometry with different codes proved this fact /6/. On the other hand the simpler formulation of the FLUT code assures a wider generality and can better cope with this new geometrical configurations /11/. The one dimensional heat conduction model of the code is able to simulate plates and hollow or full cylinders. Each heat conductor can have up to three material zones separated by gaps. Heat generation can be considered in material zones. Suitable heat transfer correlations depending on the flow regime connect the fluid and the heat conductor model. The positions of the lower and upper quench-front for each fuel rod is calculated explicitly by means of analitical correlations for the quench front velocity /12/ /13/. This compensates partly the lack of the axial conduction in the one dimensional heat conductor model.

For the simulation of a reactor primary system, a network of one dimensional flow elements (pipes) and special plenum cells (lumps) is applied. The reactor core may comprise parallel cells with fuel rods of different power connected to each flow channel. For the primary coolant pumps, a centrifugal pump model is available. The temperatures of the secondary side of the steam generator tubes and the injected mass flow rates of the ECCS must be given by input data.

The new version FLUT-FDWR contains some new correlations and physical models which improved its prevision capability /4/.

The criterion of Hsu and Young for the onset of the quench-front /14/ was introduced in order to avoid a too early quenching of the rod cladding from above. This criterion allows the beginning of the rewettig process only when the void fraction a is less then 0.95 and the cladding temperature T_{cl} is lower then 540°C and gave satisfactory results when applied in some cases in PWR geometry /15/.

A new droplet model for the zone immediately downstream the lower quench-front improved the calculation of the precooling effect in the cases in which the quenching of the cladding takes place at a high void fraction ($a \geq 0.8$ at the quench-front). Figure 1 on page 13 shows the flow patterns of the two extreme reflooding situations: flow pattern A occurs usually for high flooding rates (more then 4 cm/s) while flow pattern B is typical of low flooding rates /16/. The establishment of one or the other of these flow patterns is also affected by the inlet subcooling of the flooding water and by the volumetric power density in the bundle: lower inlet subcooling and high power density support the pattern B. In an APWR core, where the power density is higher than in a PWR, pattern B may become of major importance.

The original package of heat transfer correlations of the FLUT code is based on a flow pattern of type A and underestimates the precooling of the cladding before quenching in case of pattern B, where the zone of the dispersed flow film boiling begins directly above the quench-front. A very important parameter in this flow regime is the average droplet diameter used to calculate the heat transfer coefficient and the interfacial area between vapour and water droplets. In the original version of FLUT this parameter was set to a unique constant value. Basing on a study of R. Lee about droplet generation at the quench-front and their subsequent evolution /17/, a simplified model was implemented in FLUT-FDWR. Here the region of dispersed flow is divided into two subregions (see Figure 1 on page 13):

a zone of length L, immediately downstream the quench-front, in which the calculation uses a value $d_1 = 0.127$ mm for the droplet average diameter, accounting for the presence in this subregion of two kinds of droplets generated below (in the zone of transition boiling) by the bursting of bubbles;

the remaining part of the dispersed flow region, in which the value $d_2 = 2$ mm is used as in the original version of the program (in this zone only the bigger droplets survive, as the smaller ones evaporate completely within the first zone of length L).

For the length of the zone in which the diameter d_1 is used a reference value $L_0 = 0.2$ m was determined by means of optimisation calculations of the experiment FLECHT No. 32114. For the other cases L was calculated by means of a simplified energy balance. Supposing that the zone of influence of the small droplets depends linearly on the volumetric power density on the fluid Q and on the initial cladding superheat ΔT, referring to the value L_0 we obtain:

$$L = L_0 (Q_0/Q)(\Delta T_0/\Delta T)$$

where the values with index 0 refer to FLECHT exp. No. 32114 /5/. This simplification gave good results in the calculation of many experiments in PWR and APWR geometry /4/and was used also in the present work.

For the calculation of the friction factors, new relations for a properly evaluation in APWR core channels were introduced in FLUT-FDWR /4/.

The dependence of the interfacial drag coefficient on the channel geometry may be accounted for in FLUT-FDWR by giving different values of the parameters R_v and R_l of the relation of Oseen /18/ in the different component of a system. According to the results of parametric calculations of many reflooding experiments and to the experiences of other authors, we established the following reference values in a previous work /4/:

$R_v = R_l = 0.70$ m for avery tight APWR rod lattice (p/d = 1.06, $d_h = 2.6$ mm)

$R_v = R_l = 0.25$ m for a PWR geometry (square rod lattice with $d_h \simeq 12.0$ mm)

$R_v = R_l = 0.10$ m for pipes.

3. The Reflooding Experiments in the NEPTUN-III Facility

The NEPTUN-III Facility consists of 37 electrically heated 10.7-mm-diameter rods (Figure 2 on page 14) arranged in a triangular lattice with a pitch-to-diameter (p/d) ratio of 1.13 (Figure 3 on page 15). Each rod is 1940 mm in total length, of which 1680 mm is heated with a cosine-shaped power distribution (Figure 4 on page 15). Clad surface temperatures are measured at various elevations as indicated in Figure 3 on page 15 by level numbers. The test conditions taken from

/7/ and /9/ are listed in Table 1 on page 5. All the tests were performed with constant flooding rate and rod-power.

Test No.	Q (kW)	$T_{cl}(°C)$	$v_{fl}(cm/s)$	p (bar)	$\Delta T_{sub}(°C)$
APWR1	2.45	757	10	4.1	80
APWR2	1.19	757	4.5	4.1	80
APWR3	1.19	597	4.5	4.1	80
APWR4	1.19	477	4.5	4.1	80
APWR5	2.45	597	4.5	4.1	80
APWR6	1.19	757	10	4.1	80
APWR7	1.19	757	15	4.1	80
APWR8	1.19	597	2.5	4.1	80

Table 1.   Main Forced Reflooding Test Data: The data for the first 7 tests are taken from /7/. The 8th test was object of a pre-test calculation and the corresponding data are taken from /9/.

4. Nodalisation and Calculation Option

Figure 5 on page 16 shows the nodalisation used for the calculations. The test section was simulated by means of an 8-cell pipe connected to a group of 43 conductors representing the 37 rods-bundle. The lower and upper plena of the facility are simulated by 2 lumps. The injection of the reflooding water takes place in the lump-cell L1 (lower plenum) while the upper plenum L2 is imposed a condition of constant pressure. The first cell of the pipe has a length of 200 mm and is connected with a single conductor simulating the cold end of the rod-bundle. Each one of the other seven 240 mm long cells is coupled with 6 conductor segments simulating the heated part of the rods.

The radial discretisation of the conductor segments was a problem for these calculations. As mentioned in Chapter 2 the conduction model of the FLUT-Code can

account for a maximum of three different material zones per segment, separated by gaps. The complicated radial geometry of the NEPTUN fuel rod (see Figure 2 on page 14) cannot be represented precisely using this model. Beginning from the center, the first material zone must be used for representing the kanthal-heater and the third one for the simulation of the inconel-cladding. The remaining second zone must then comprehend the boron insulation and other four layers respectively of inconel, cupper, inconel and aluminium-oxide. For this zone a pseudo-material was used, whose physical properties were obtained averaging the properties of the real materials taken from Ref. /9/. The density and heat capacity values were averaged on the volume and mass of the corresponding material respectively. For the heat conductivity a logarithmic average on the layers-diameter was used, taking into account also the thermal resistence of the contact surfaces between different materials.

This method had already been used by the author with satisfactory results /19/.

All the calculations were performed using the droplet model shortly described in Chapter 2. For the droplet diameters d_1 and d_2 the standard values mentioned above were adopted in all cases. For the length L the equation of Chapter 2 gave results greater then the limit value 0.2 m in all the cases with lower power. Here the limit value was used in the calculations. For the two tests with higher rod power, APWR1 and APWR5 in Tab. 1, values of 0.1273 m and 0.1723 m respectively were calculated.

The geometric parameters for the interfacial drag coefficient were determined for the NEPTUN-III test scection by means of a linear interpolation on the hydraulic diameter of the values for the PWR and for the APWR case given above. Having a hydraulic diameter of 4.17 mm we obtain for R_v and R_l a value of 0.62 m.

For the wall friction factors the correlation of Cheng and Todreas for the laminar flow and that of Koo-Drew-Mc Adams with the correction factor of Baxi-Dalle Donne for turbulent flow were chosen /5/.

The pressure loss due to the grid spacers was taken into account by means of constant form loss coefficients given as input.

5. Results

Table 2 shows the main results of the calculations. For the first 7 tests the calculated quench-time of the 4[th]level is compared with the measured value taken from /7/ and we can notice a good agreement.

Test No.	t_{q4} (s) (measured)	t_{q4} (s) (calculated)	collapsed liquid level(m) (calculated)	T_{max} (°C) (calculated)	Turn around time (s) (calculated)
APWR1	109	93	0.88	812	44
APWR2	109-114	112	1.06	769	54
APWR3	82-86	92	1.06	618	55
APWR4	55-61	69	1.03	499	17
APWR5	142-148	141	0.81	714	73
APWR6	84	77	1.14	766	31
APWR7	62	65	1.14	766	25
APWR8	-	127	0.89	666	76

Table 2.   Main Results of Calculations.:   The collapsed liquid level reported in this table is calculated at the time at which level 4 is quenched (see t_{q4} calculated). The measured quench time for the fourth level is also given for comparison.

A more complete comparison of the computed and measured quench-front progression can be seen in Figure 6 on page 16 to Figure 12 on page 19. Satisfactory results were obtained in all cases for the lower quench-front, while for the upper quench-front a too high velocity was computed, especially for the tests with a high flooding rate (APWR1, APWR6 and APWR7). For the test No. 1, for which no upper quench-front was detected during the experiment, a second calculation was performed in which the upper quench-front velocity was set to zero. In Figure 6 on page 16 this is labelled as 'Calculation NQ'. The figure shows that even without a quench-front from the top, the upper part of the rod is rewetted too early, as a too

high velocity of the lower quench-front is calculated for it. For the test No. 1 we can compare with the experimental data from /7/also the cladding temperatures computed for the mesurement levels 3, 4 and 5 (see Figure 3 on page 15). Figure 13 on page 20 (cladding temperature at level 3) shows a good agreement of both calculations with the experiment. At the 4th level (Figure 14 on page 20) the quench-temperature (temperature at which the quenching phenomenon begins) and the quench-time are still good evaluated in the calculations, but the overall trend differs from the measurement. In Figure 15 on page 21 (5th level) the curve calculated with the standard options of FLUT-FDWR differs considerably from the measured values. The quench temperature corresponds to the measured one, but rewetting takes place 47 s before then in the experiment, because of the upper quench-front calculated by the code (see also Figure 6 on page 16). In the calculation NQ, where the upper quench-front was eliminated, the results are better, but the rewetting of the 5th level takes place still 18 s too early, because of the too high velocity of the lower quench-front (see Figure 6 on page 16). The temperature trend shows another peculiarity of the FLUT-calculations. The computed curves at all three levels have small oscillations with no correspondence in the measurements. They are due to the strong oscillations of the fluid-temperature (see Figure 16 on page 21). This problem is present also in all the other calculations reported here (see Figure 17 on page 22 to Figure 22 on page 24[2]) and was already noticed also in previous calculations /19/. Due to the lack of axial conduction the position of the quench-front must be determined by means of a quench-velocity model. As the quench-front advances from one segment to another the heat flux from cladding to liquid reaches peak values. This produces a strong oscillating evaporation rate in the fluid cell containing the quench-front and consequently the oscillations of the vapour temperature in the zone above. The frequency of these oscillations depends directly on the discretisation of the heater rod and of the flow-channel.

Fot the test No. 8 no experimental data are yet available for comparison. In Figure 23 on page 25 to Figure 27 on page 27 the main results of the standard FLUT-FDWR calculation, named calculation 1 (see the nodalisation description and calculation options described in Chapter 4), are compared with a second calculation for which a finer discretisation of the fluid channel was used. The first cell of the flow channel (see Figure 5 on page 16) and the corresponding heater

---

[2] For the experiments No. 2 to 7 no experimental data about cladding temperatures were available and only the computed cladding and vapour temperatures at the 4th level are reported in the figures.

segment (cold end of the heater rod) were divided into two parts. Every other cell was divided into three parts leaving the heater segments unchanged, so that in the new nodalisation every cell of the heated part is connected with only two heater segments instead of six as in the first one. Altogether the new nodalisation comprehends 23 fluid cells and 44 heater segments.

In Figure 23 on page 25 the lower quench-front of the second calculation advances slightly quicker than in the first one (standard case), due to a higher collapsed liquid level (see Figure 24 on page 25). Owing to the finer discretisation of the fluid cells, the progression of the collapsed liquid level is more regular in calculation 2 and the carry over becomes smaller (see Figure 25 on page 26). On the other, hand the parameters R_v and R_l for the calculation of the interfacial drag coefficient had been optimized for a coarser mesh /19/ and are probably too high for the finer discretisation. Anyway the calculated maximum cladding temperatures for the 4th level are almost equal in the two cases (see Figure 26 on page 26 and Figure 27 on page 27), though the general trend is much more regular in the second calculation.

6. Conclusions

The limited comparison of the results of the calculations with the experimental data confirms the capability of the program to satisfactory compute the advancement of the lower quench front in an APWR bundle. On the other hand, most calculations show a too quick progression of the upper quench front.

The oscillating trend of the computed vapour and cladding temperatures for all tests points out the need of further improvements in the calculation of the heat transfer form cladding to fluid in the cell containing the quench front.

The differences in the results of the two pretest calculations performed for the test No. 8 show the importance of the nodalisation effect for the determination of the values of the empirical parameters used by the code.
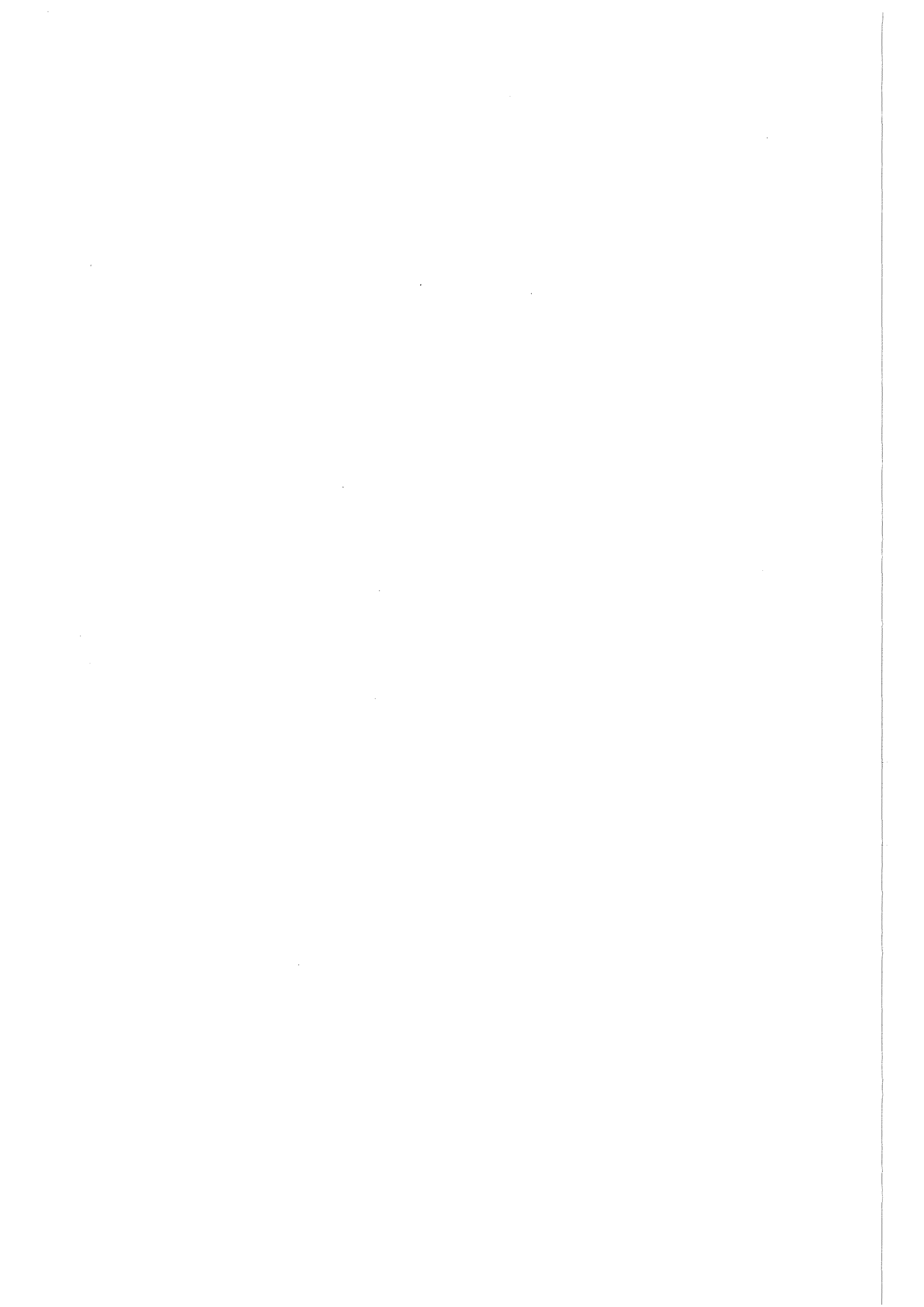
References

/1/ H.STAEDTKE and W.KOLAR, "Predictions Capabilities of RELAP5/Mod1-EUR; An Improved Version of the LWR Safety Code RELAP5/Mod1," Trans. 4th Int. ENS/ANS Conf. and 9th Foratom Congress (ENC '86) Nuclear Energy of Today and Tomorrow, Geneva, Switzerland, June 1-6, 1986.

/2/ V.TESCHENDORFF, "The Two Fluid Code FLUT for LOCA Reflood Analysis," presented at Workshop International Atomic Energy Agency Program in Uses of Computer Codes for Safety Analysis, Varna, Bulgaria, (May 1984).

/3/ M.DALLE DONNE and C.FERRERO, "Loss-of-Coolant-Accident and Anticipated Transient without SCRAM Calculations for Homogeneous and Heterogeneous Advanced Pressurized Water Reactors," Nucl. Technol. 80, 133 (1988).

/4/ M.CIGARINI and M.DALLE DONNE, "The Reflooding Phase after a Loss -of-Coolant Accident in an Advanced Pressurized Water Reactor," Nucl. Technol. 84, 33 (1988).

/5/ M.CIGARINI, internal KfK-report, (1989).

/6/ F.J.ERBACHER and K.WIEHR, "Experimental Investigation on Reflooding and Deformation Behaviour of an APWR Tight Lattice Fuel Rod Bundle in a LOCA," Nucl. Technol. 80, 153 (1988).

/7/ J.DREIER et al., "Experimental Simulation of LOCA Reflooding Conditions for Light Water High Converter Reactors," Proc. 4th European Nuclear Conf. and 9th Foratom Congress (ENC 86) on Nuclear Energy, Geneva, Switzerland, June 1, 1986, Vol. 2, p. 575, European Nuclear Society (1986).

/8/ J.DREIER, G.ANALYTIS and R.CHAWLA, "NEPTUN-III Reflooding and Boiloff Experiments with an LWHCR Fuel Bundle Simulator: Experimental Results and Initial Code Assessment Efforts," Nucl. Technol. 80, 93 (1988).

/9/ J.DREIER, not published report, Paul Scherrer Institut, Würenlingen, (1988).

/10/ A.HORA,CH.MICHETSCHLÄGER,H.G.SONNENBURG,V.TESCHENDORFF, "Analysis of Reflood Phenomena by the Two Fluid Code FLUT," NATO Advanced Research Workshop Spitzingsee/Schliersee, (Aug.31-Sept.3 1982).

/11/ M.CIGARINI, "Vorausberechnung des ersten FDWR-Flutexperimentes mit dem FLUT-Rechenprogramm," PNS-Jahresbericht 1986, pp. 4100-97, KfK 4100, Karlsruhe, (1987).

/12/ R.SEMERIA and B.MARTINET, "Calefaction Spots on a Heating Wall: Temperature Distribution and Resorption," Proc. Inst. Mech. Engr.,180, 192, (1966).

/13/ A.YAMANOUCHI, "Effect of Spray Cooling in Transient State after Loss of Coolant Accident," Journ. of Nucl. Sci. and Tecn., 5(11), 547, (1968).

/14/ Y.Y.HSU and M.W.YOUNG, "A Criterion for the Onset of Quench for Low Flow Reflood," NUREG 0915, (1982).

/15/ M.CIGARINI, "Nachrechnung des FEBA Versuchs Nr. 216 mit dem FLUT Programm," PNS-Jahresbericht 1984, pp. 4100-61, KfK 3550, Karlsruhe, (1985).

/16/ L.E.HOCHREITER and K.RIEDLE, "Reflood Heat Transfer and Hydraulics in Pressurized Water Reactors," Symposium on the Thermal and Hydraulic Aspects of Nuclear Reactor Safety, Vol. 1, ASME, pp. 75-107, (1977).

/17/ R.LEE, "Dispersed Flow Heat Transfer above a Quench Front during Reflood in a Pressurized Water Reactor after a Large Break Loss-of-Coolant Accident," University of Maryland, Ph.D. Thesis, (1982).

/18/ C.W.OSEEN, "Neuere Methoden und Ergebnisse in der Hydrodynamik," Akademische Verlagsgesellschaft m.b.H. Leipzig, (1927).

/19/ M.CIGARINI, "Thermohydraulische Untersuchungen zu den Vorgängen wärend der Flutphase nach einem Kühlmittelverlust bei einem fortgeschrittenen Druckwasserreaktor," Dissertation TH-Karlsruhe, (1987).

Figure 1. Reflood flow regimes and droplet model.

Pattern A	Flow regimes	Pattern B	Flow regimes	The new droplet model
	Annular flow ← upper quench front		Annular flow ←upper quench front	
	Single phase vapour ←α=1		Single phase vapour ←α=1	
	Dispersed flow film boiling		Dispersed flow film boiling	simple droplet population average diameter d_2
	Inverted annular flow film boiling		←lower quench front	double droplet population average diameter d_1
	←lower quench front		Transition boiling	Bubble burst
	Transition boiling T_{CHF} Nucleate boiling		Annular flow	
			Nucleate boiling	
	Single phase liquid		Single phase liquid	

-13-

Longitudinal
(not to scale)

60

Heated length

1680

200

115

5.0
diam

Copper

O Reference line

Nickel

Kanthal

Boron

Copper

Al_2O_3

Inconel 600

Nickel

(a)

Cross sectional

8.4 diam

7.8 diam

6.2 diam

5.6 diam

Minimum 1.9 diam

Maximum 0.5 diam

Thermo-
couples

0.73 diam

9.0 diam

9.54 diam

10.0 diam

10.72 diam

0.23 diam

(b)
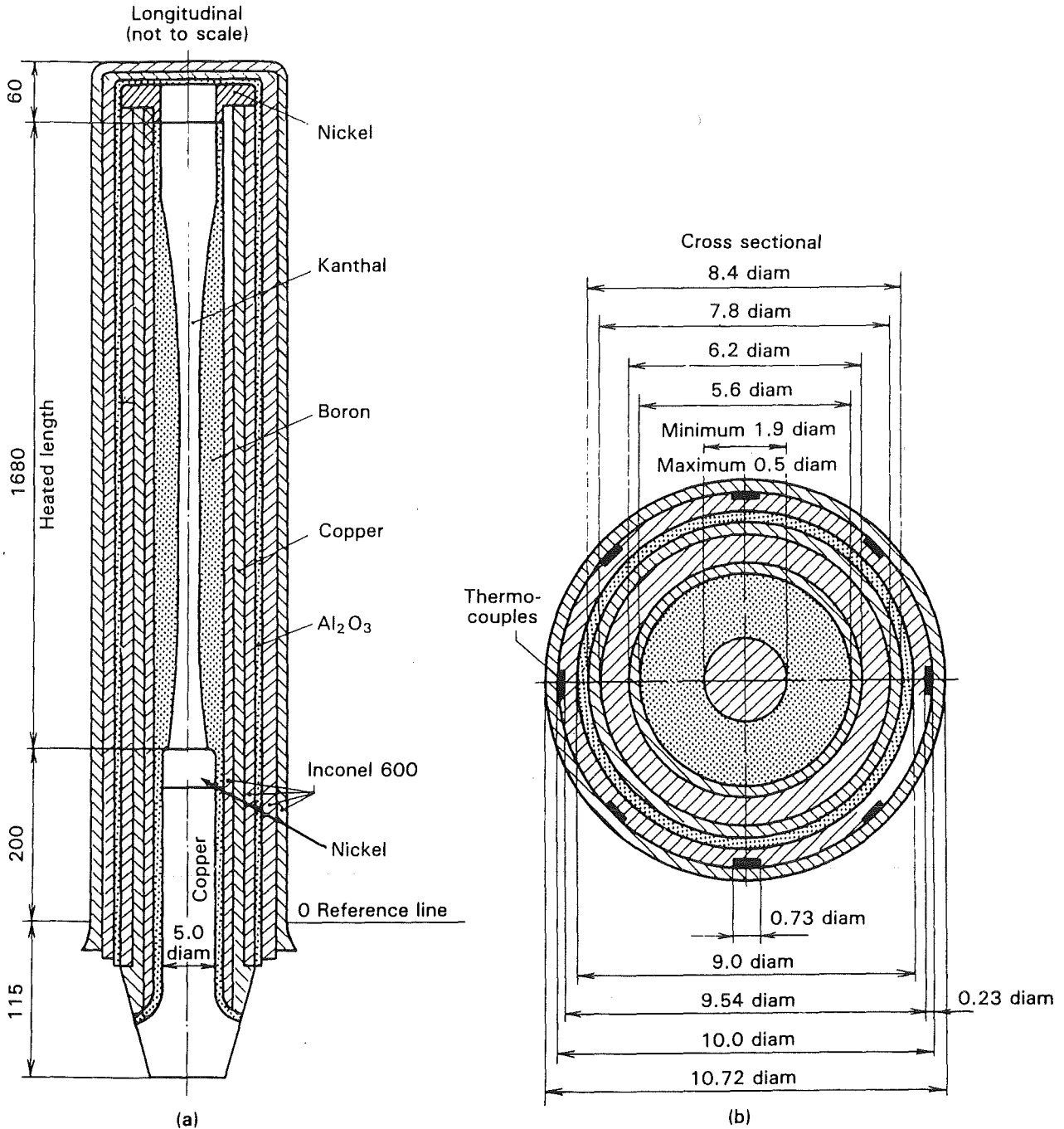
Figure 2.   Geometry of the NEPTUN heater rod: Dimensions are in millimetres.
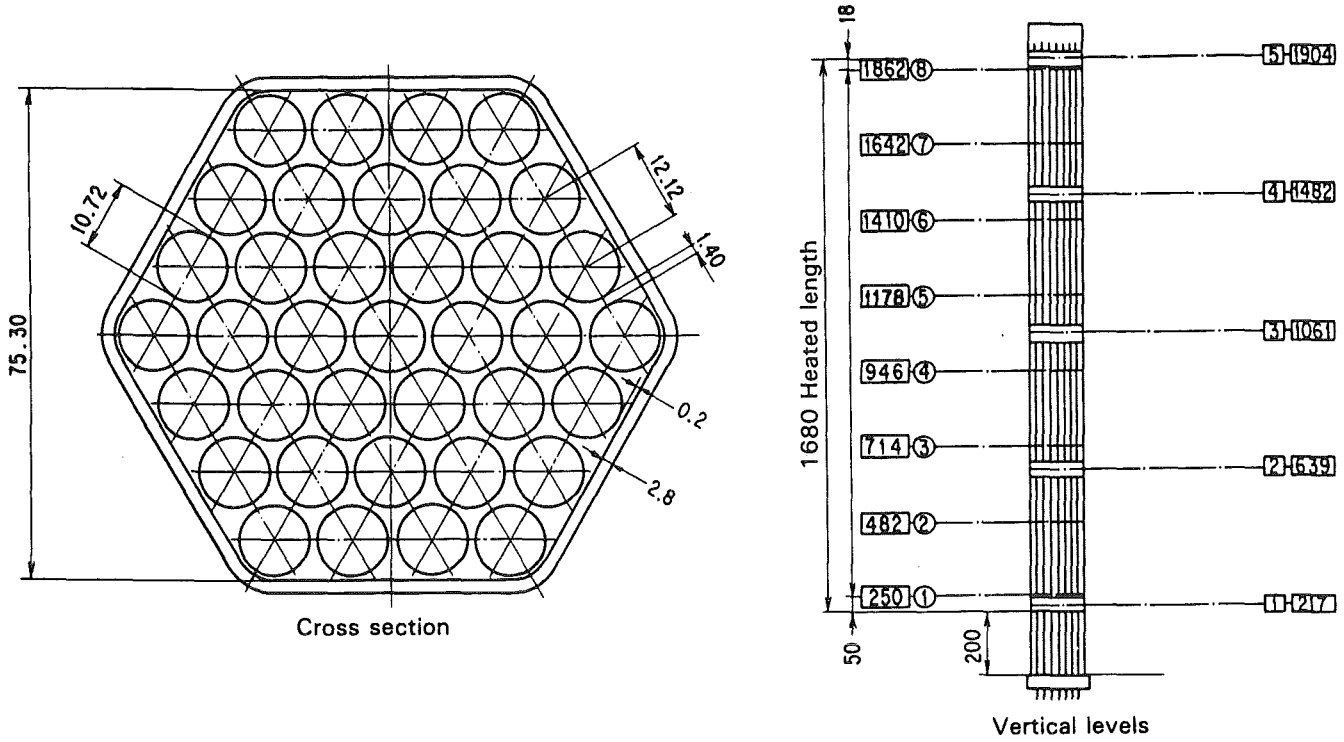
Figure 3. NEPTUN bundle: Dimensions are in millimetres.
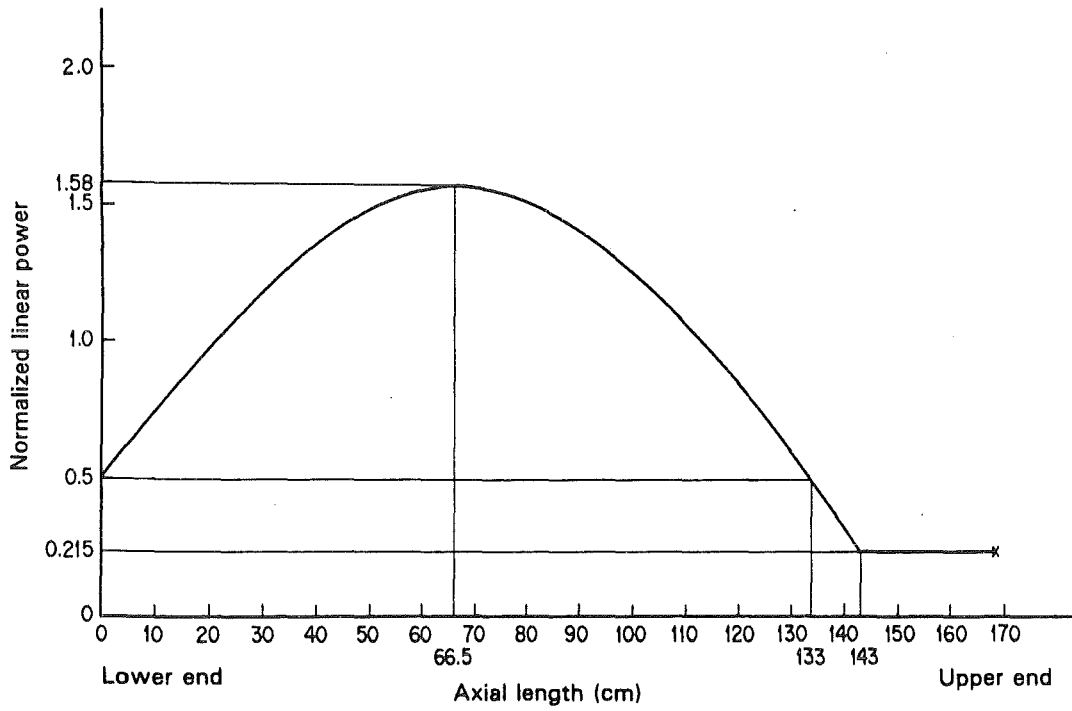
Figure 4. Axial power distribution of heater rods.

L2

#8

#7

#6

#5

#4

#3

#2

#1

L1

Components of the Nodalisation:

1 Pipe (8 fluid cells)

2 Lumps (L1 and L2)

43 Heat conductors
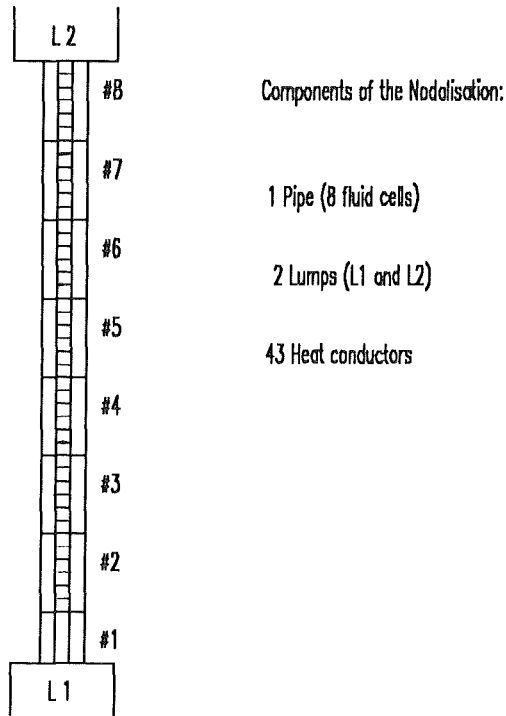
Figure 5. FLUT-Nodalisation of the NEPTUN-Test section.

□ □ Measured
—— Calculated with FLUT-FDWR (lower QF)
- - - - Calculated with FLUT-FDWR (upper QF)
· · · · Calculation NQ (lower QF)
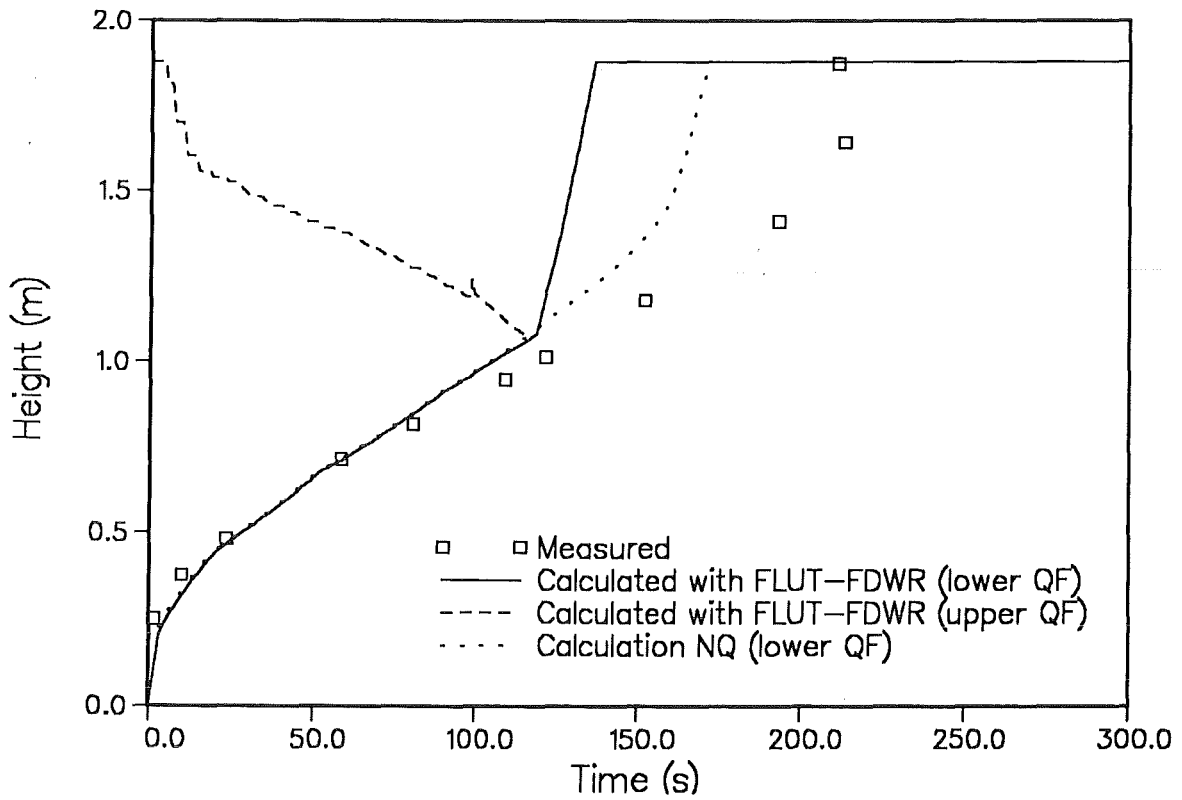
Figure 6. Test Nr. 1 - Quench-front propagation: Calculation NQ was executed excluding the upper quench-front.
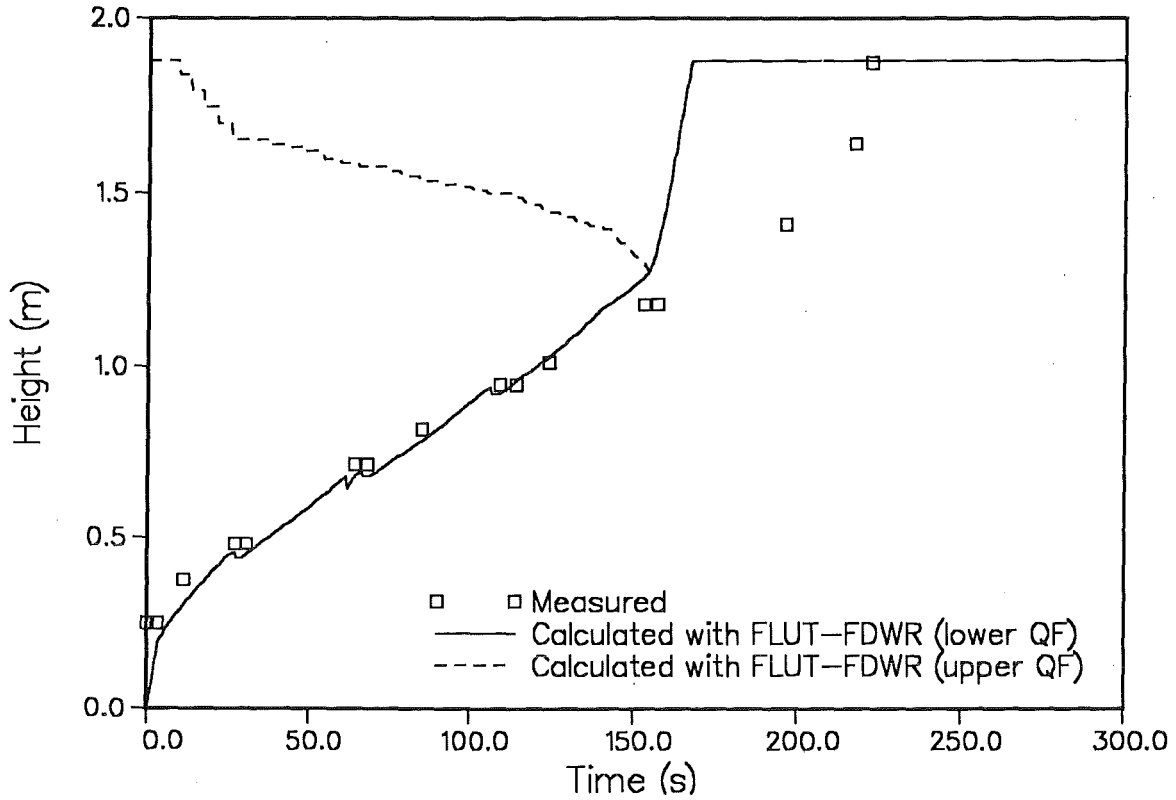
Figure 7. Test Nr. 2 - Quench-front propagation.
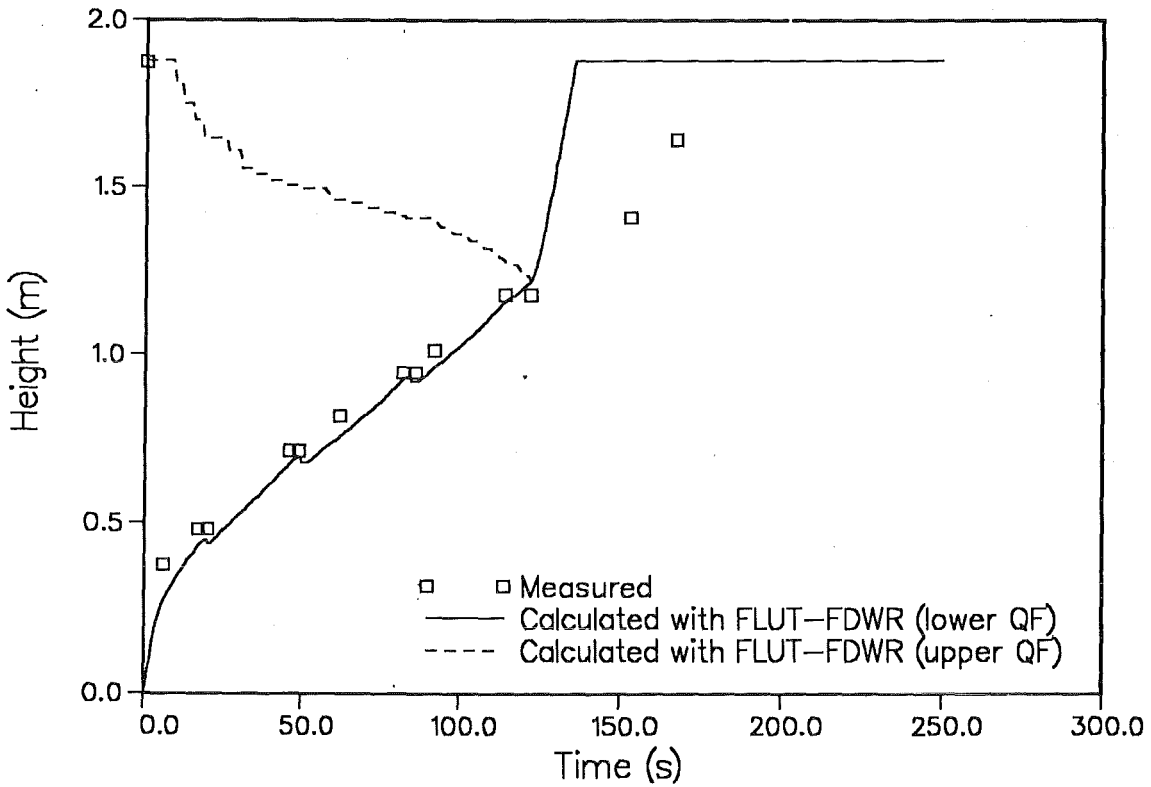
Figure 8. Test Nr. 3 - Quench-front propagation.
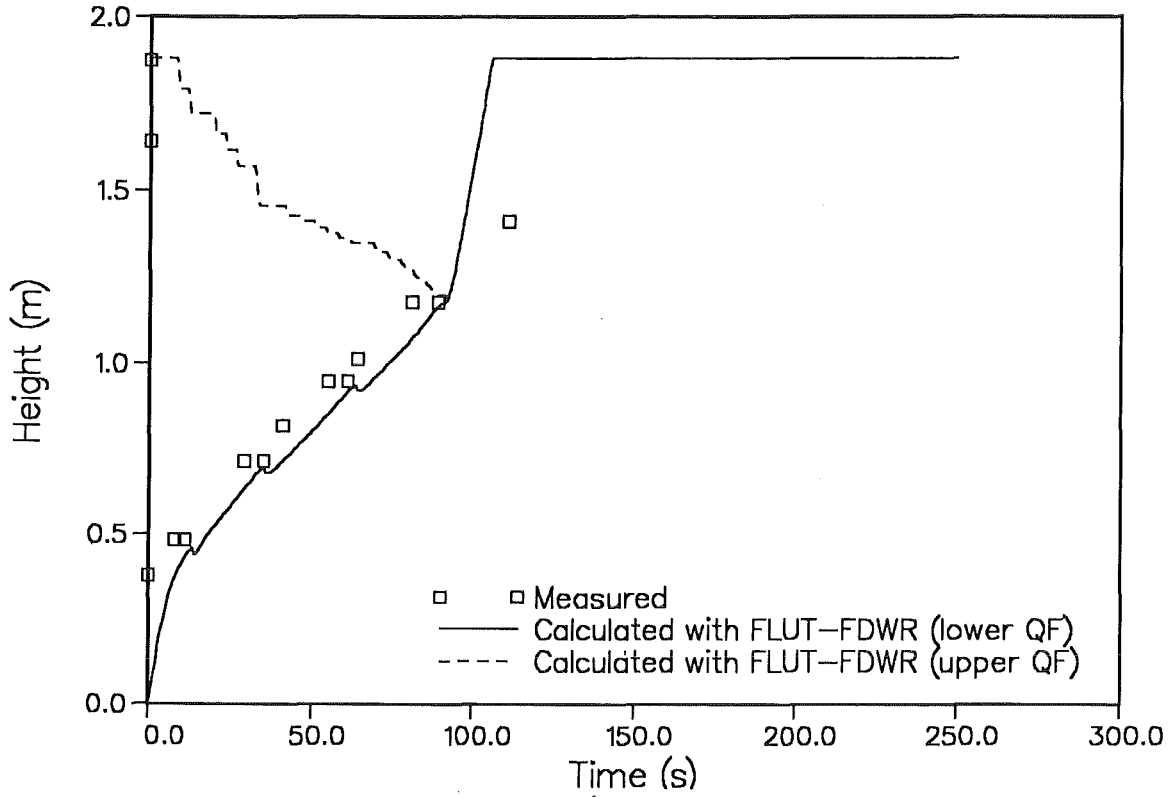
Figure 9. Test Nr. 4 - Quench-front propagation.
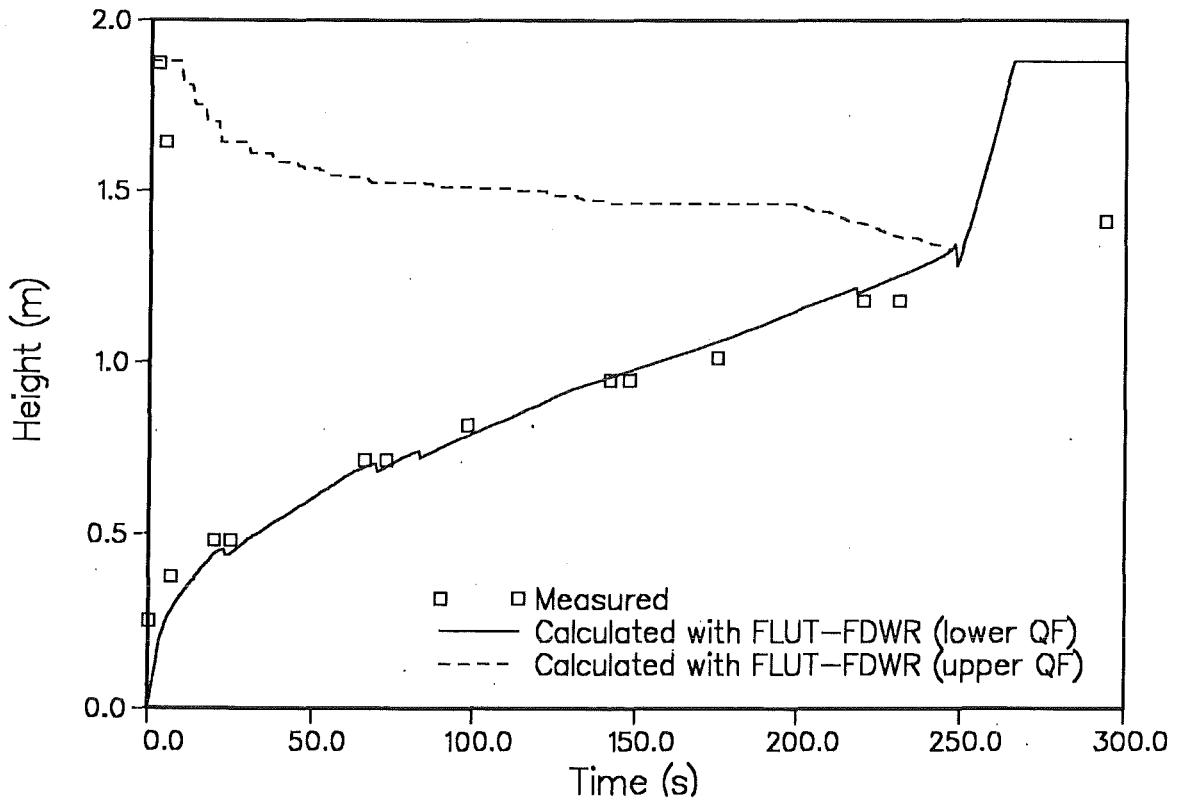
Figure 10. Test Nr. 5 - Quench-front propagation.
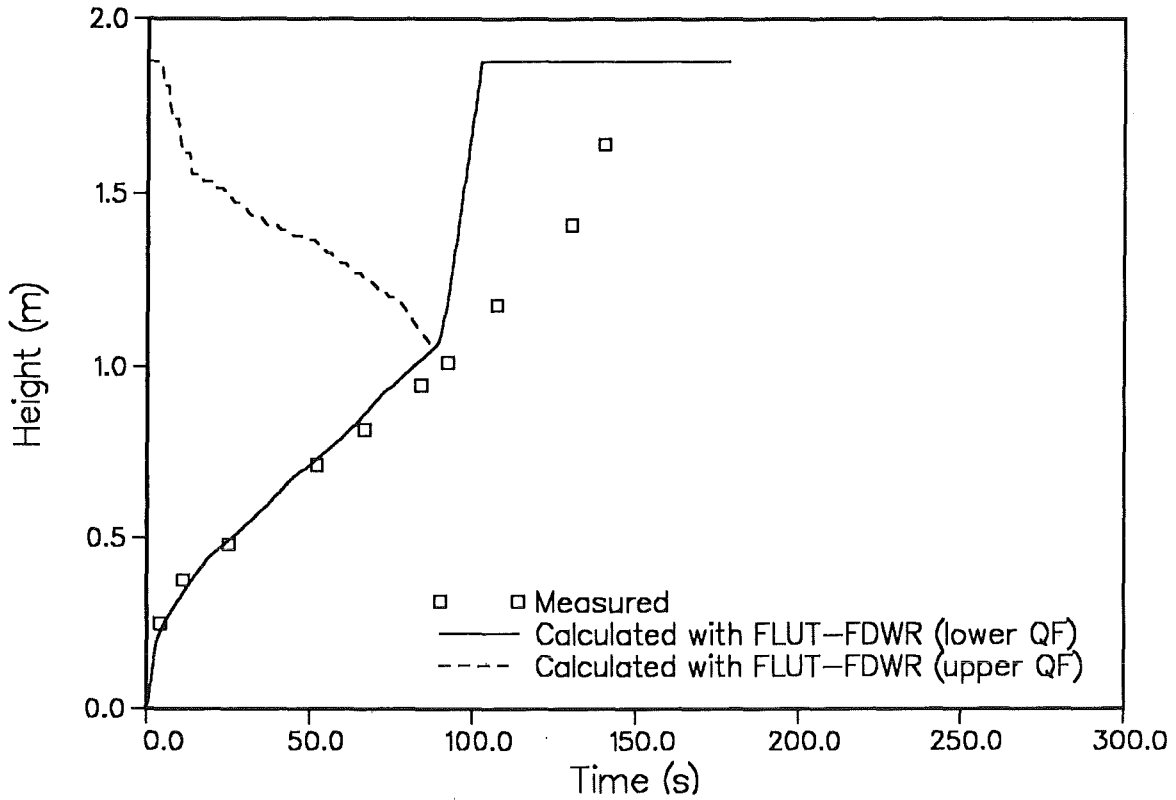
Figure 11.   Test Nr. 6 - Quench-front propagation.
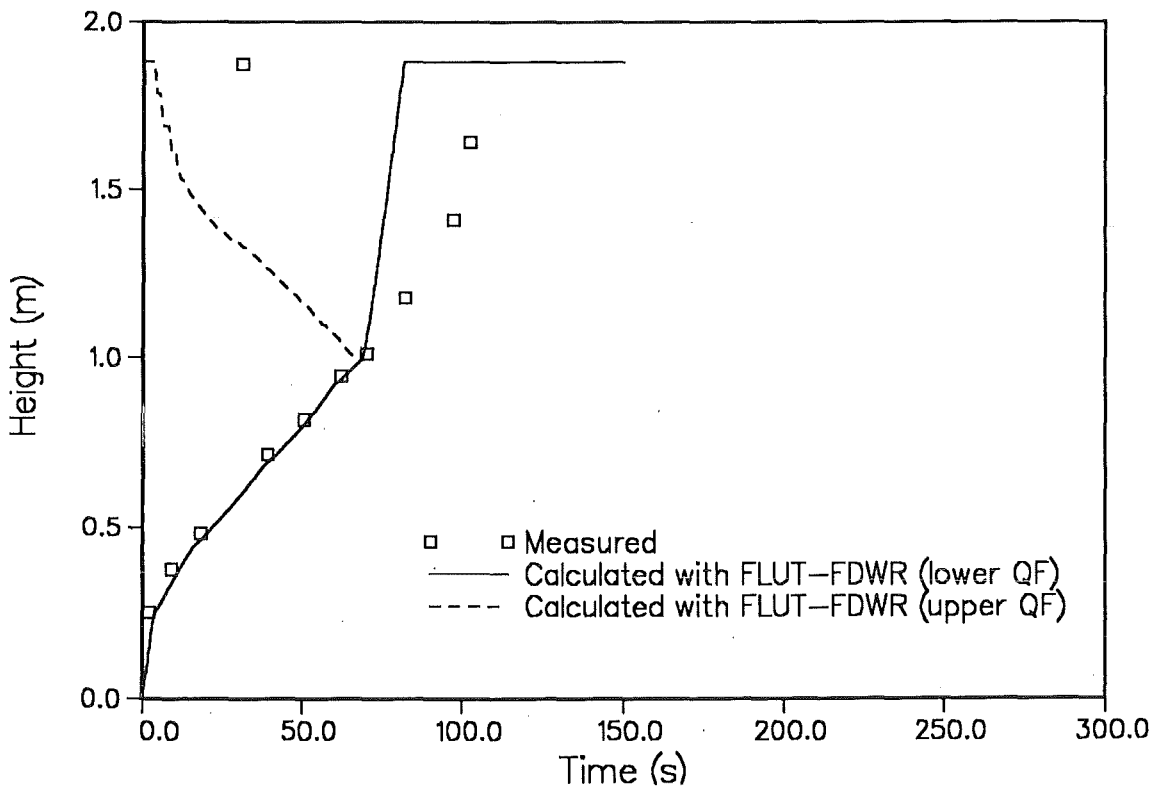
Figure 12.   Test Nr. 7 - Quench-front propagation.
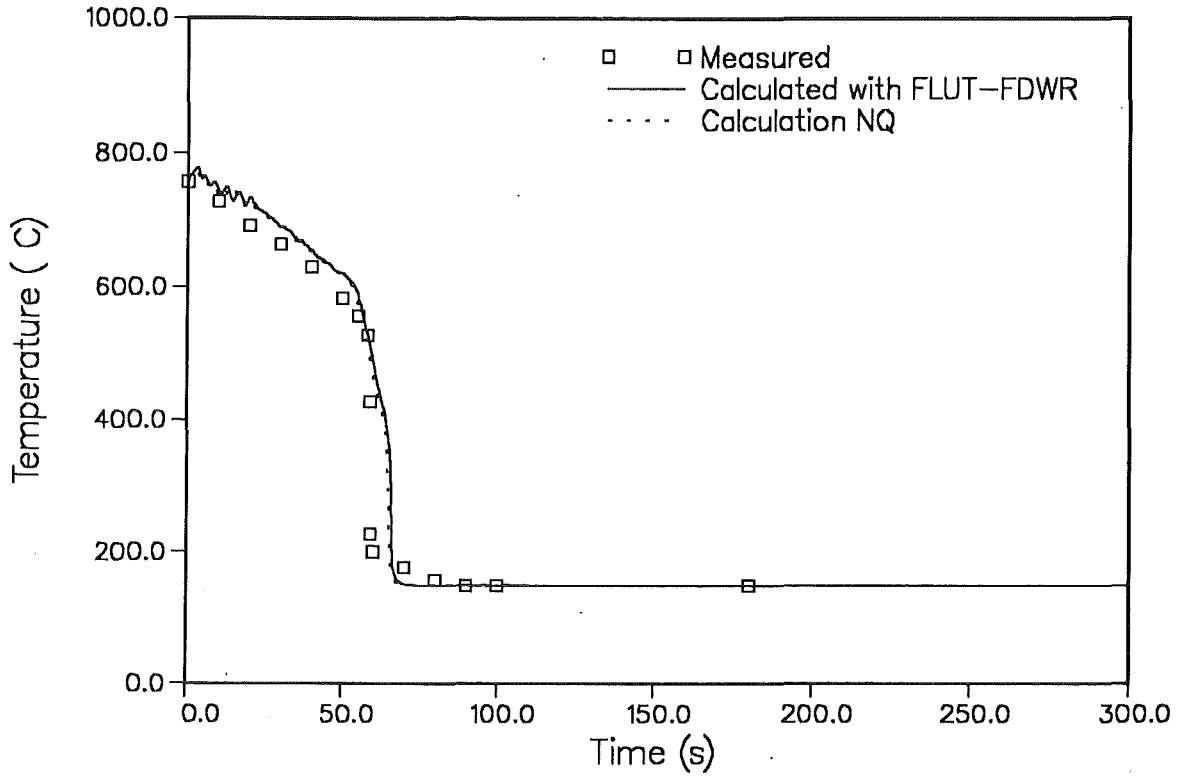
Figure 13.   Test Nr. 1 - Cladding temperatures at level 3.
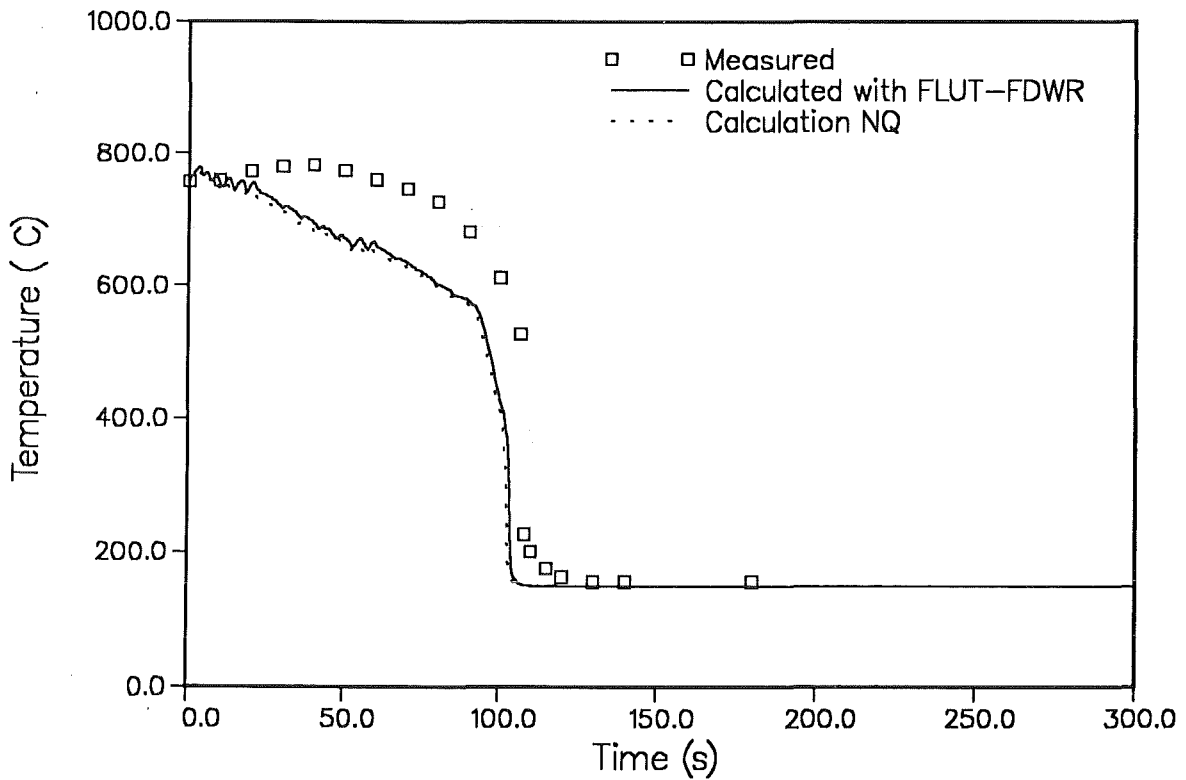
Figure 14.   Test Nr. 1 - Cladding temperatures at level 4.
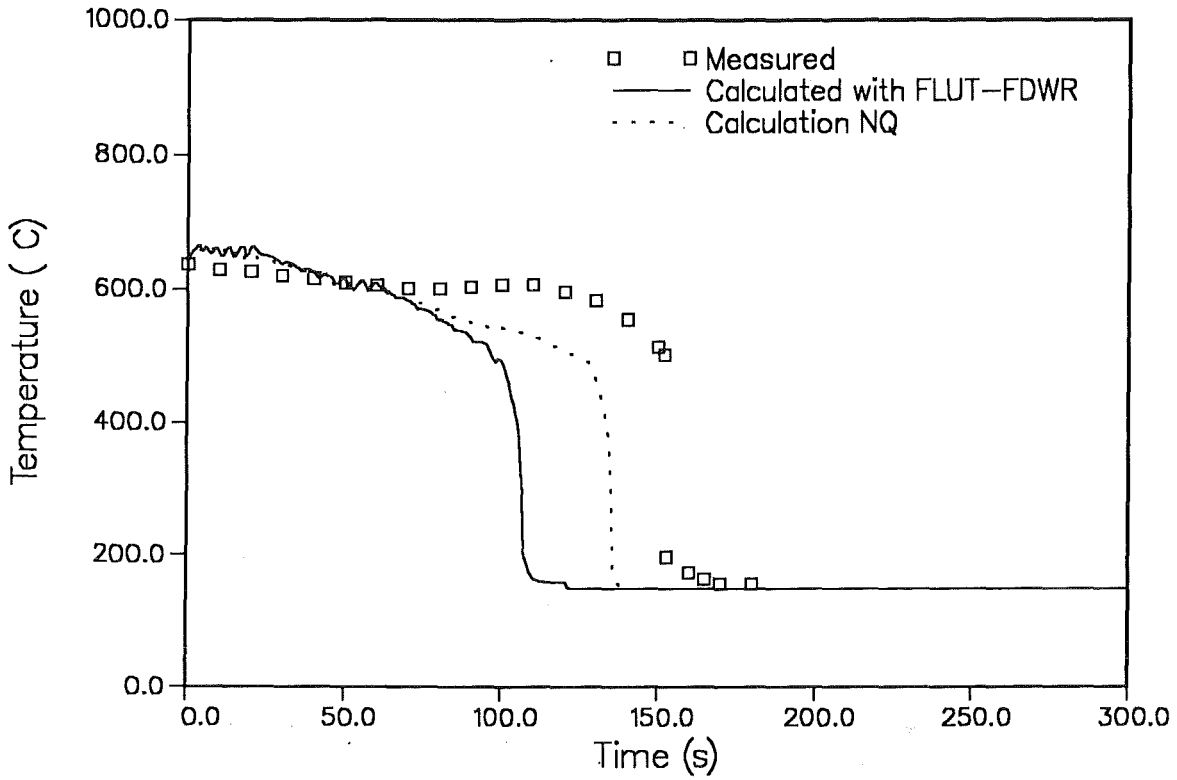
Figure 15.   Test Nr. 1 - Cladding temperatures at level 5.
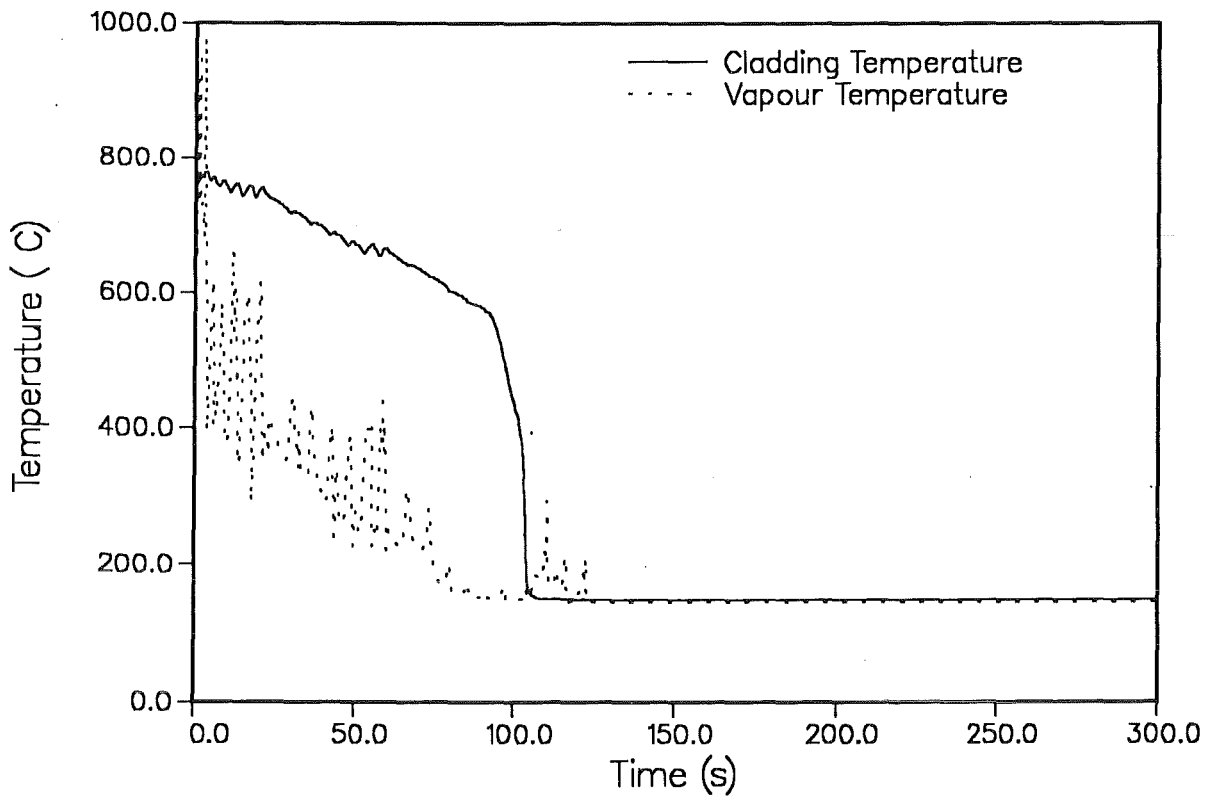
Figure 16.   Test Nr. 1 - Cladding and vapour temperatures at level 4.
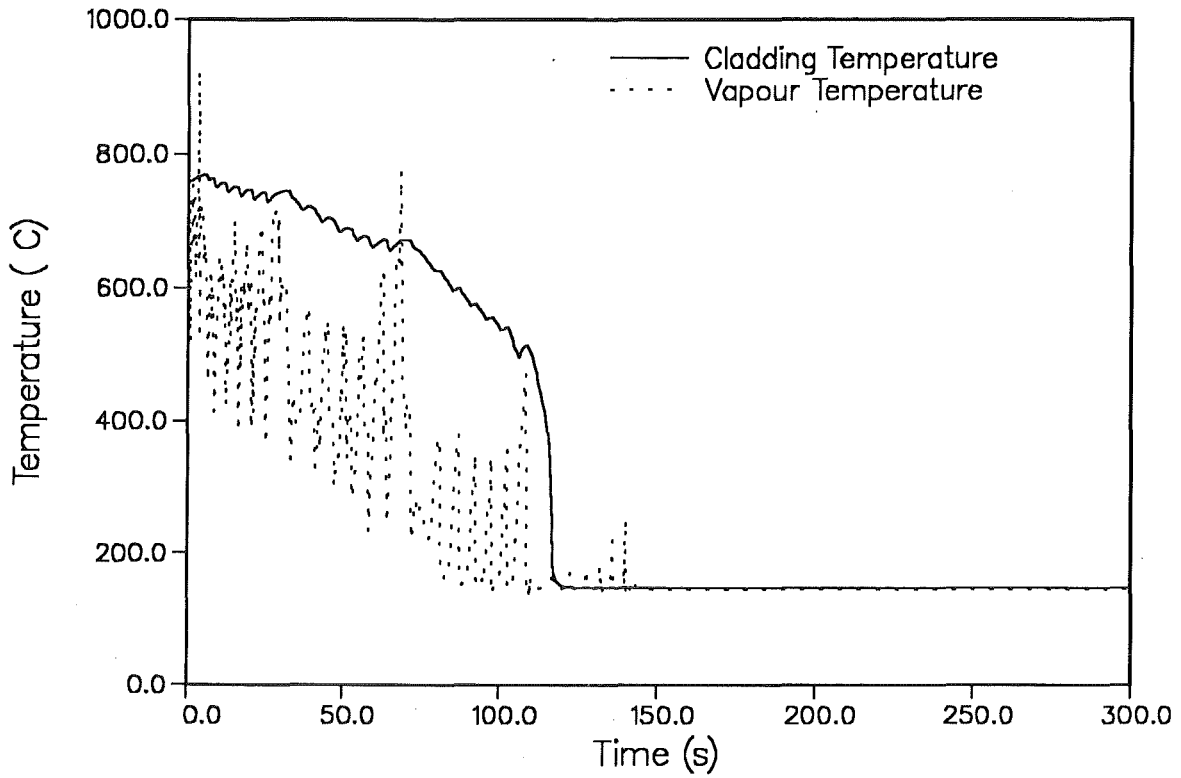
Figure 17.   Test Nr. 2 - Cladding and vapour temperatures at level 4.
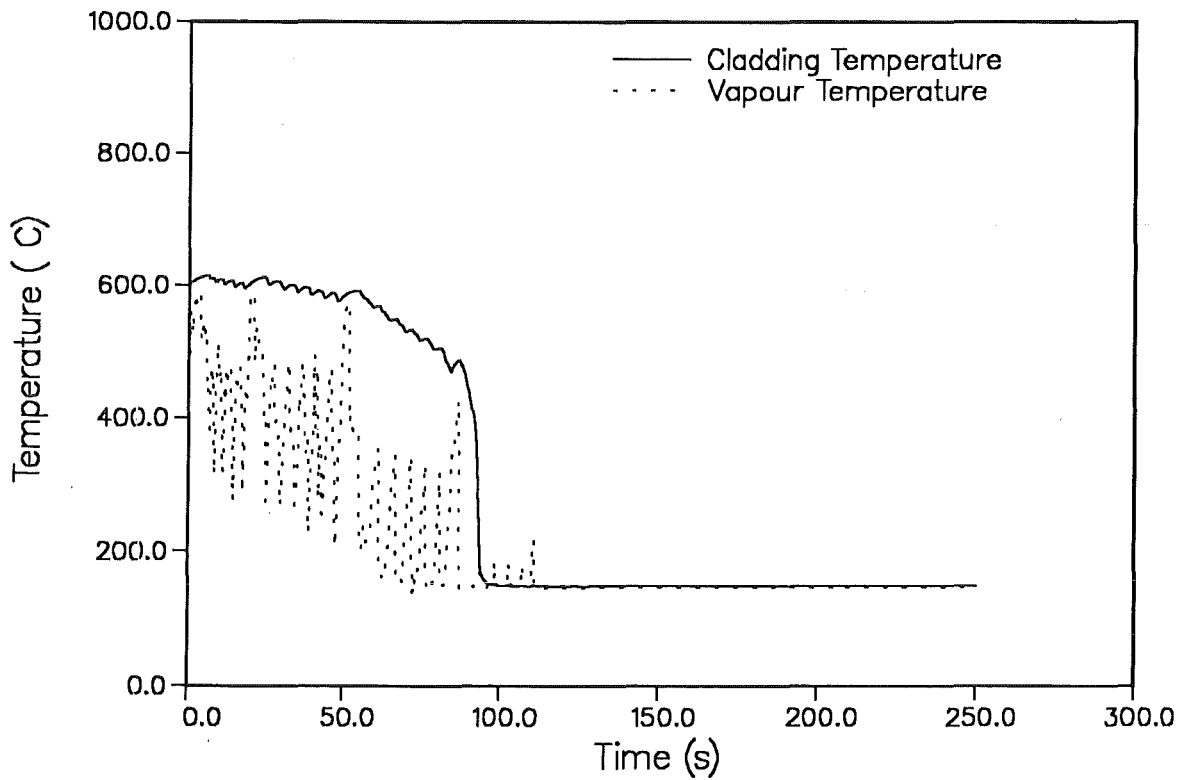
Figure 18.   Test Nr. 3 - Cladding and vapour temperatures at level 4.
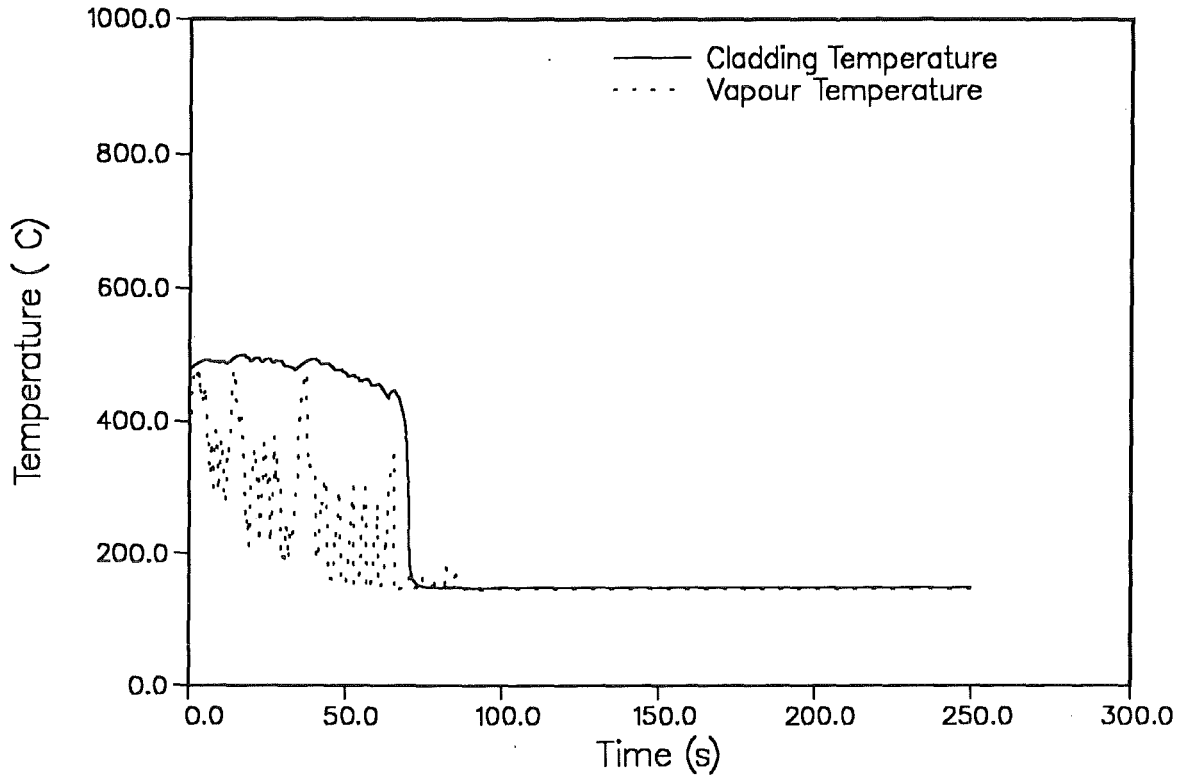
Figure 19. Test Nr. 4 - Cladding and vapour temperatures at level 4.
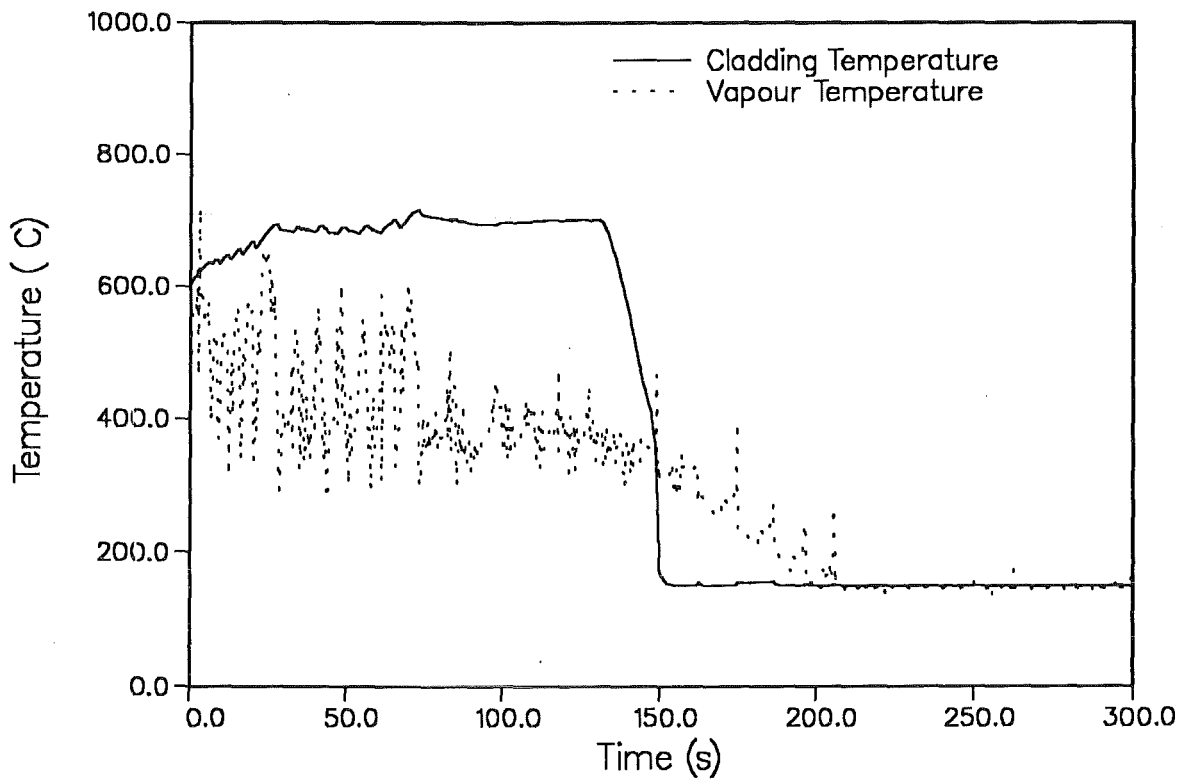
Figure 20. Test Nr. 5 - Cladding and vapour temperatures at level 4.
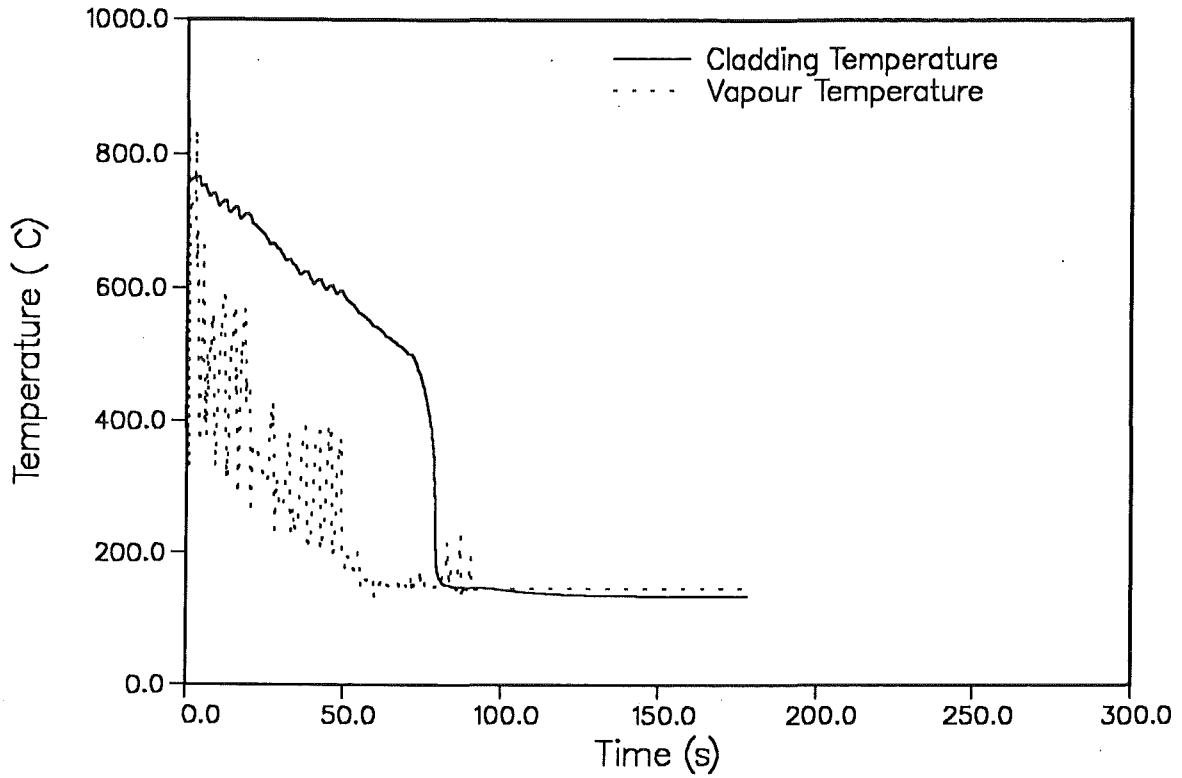
Figure 21. Test Nr. 6 - Cladding and vapour temperatures at level 4.
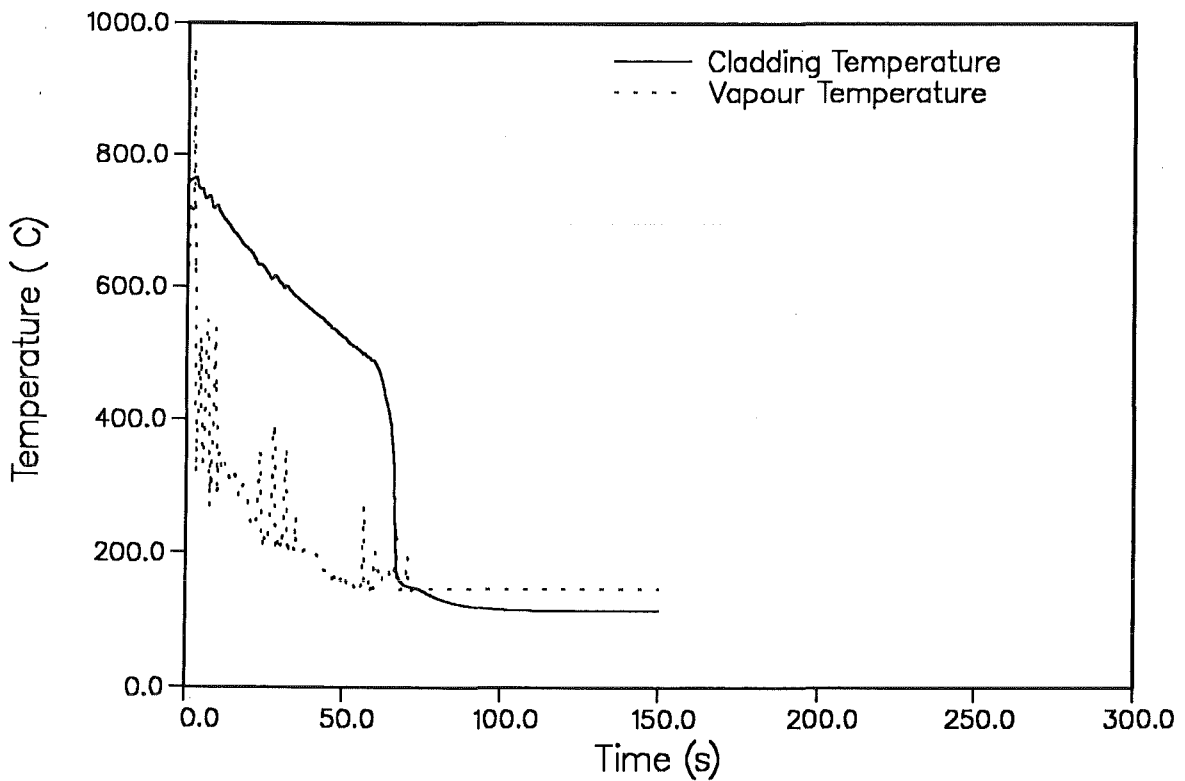
Figure 22. Test Nr. 7 - Cladding and vapour temperatures at level 4.
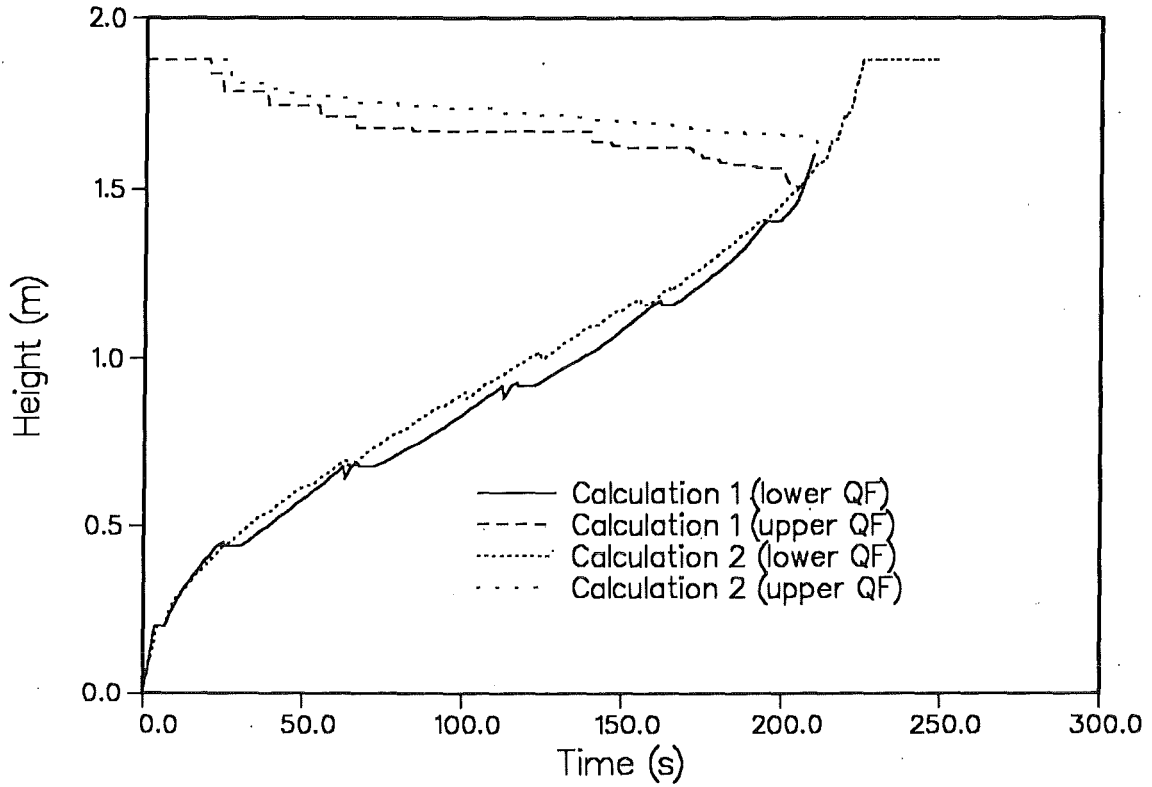
Figure 23. Test Nr. 8 - Quench-front propagation: Pre-test calculations.
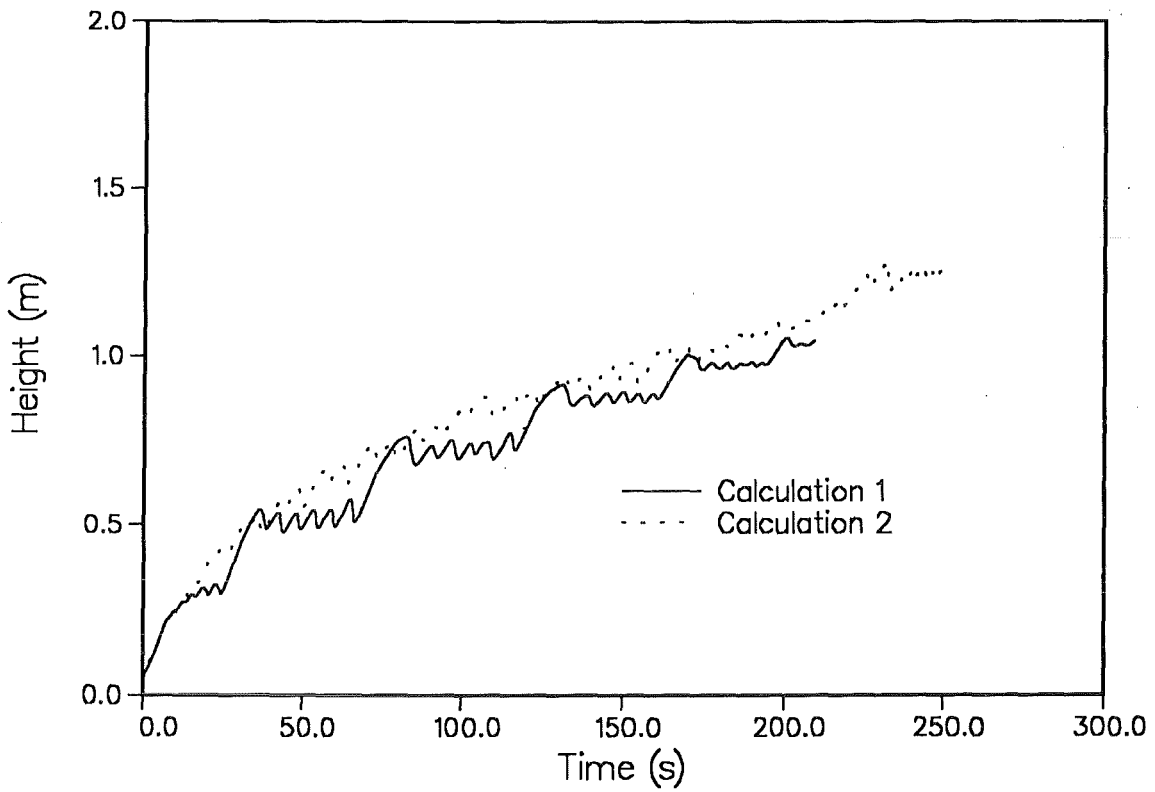
Figure 24. Test Nr. 8 - Collapsed liquid level: Pre-test calculations.
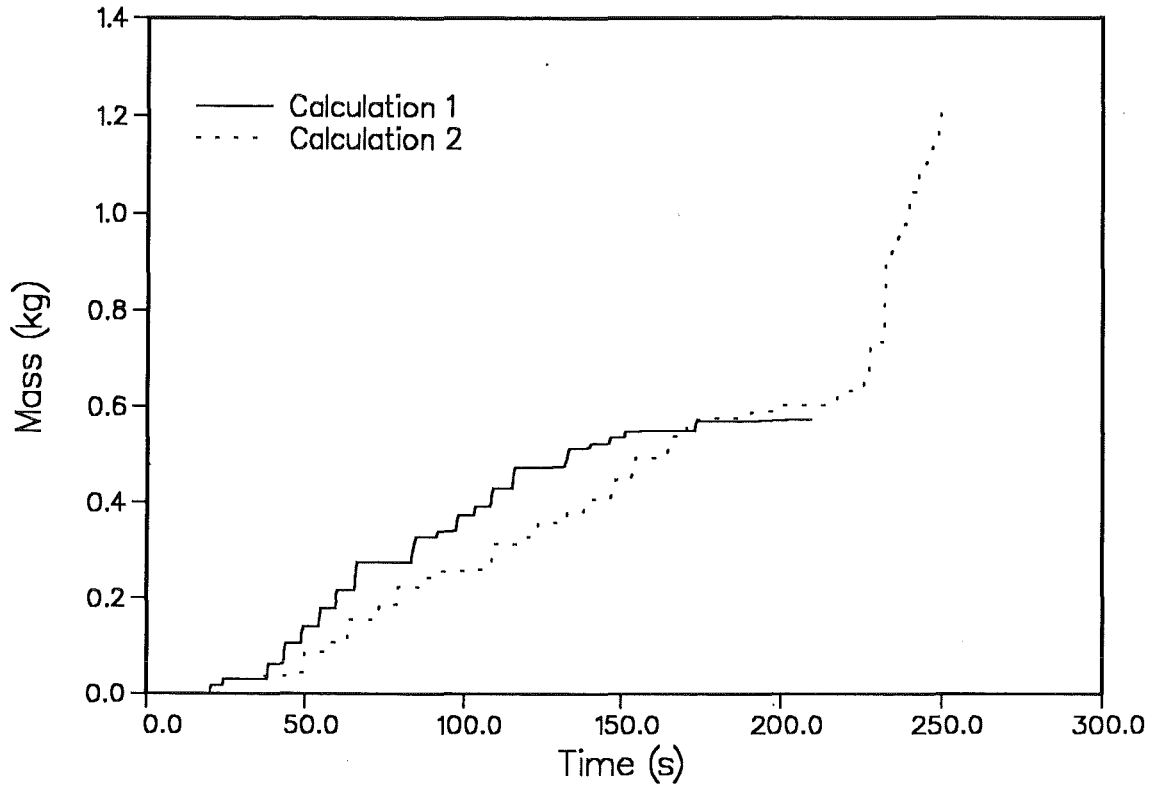
Figure 25. Test Nr. 8 - Carry over: Pre-test calculations.
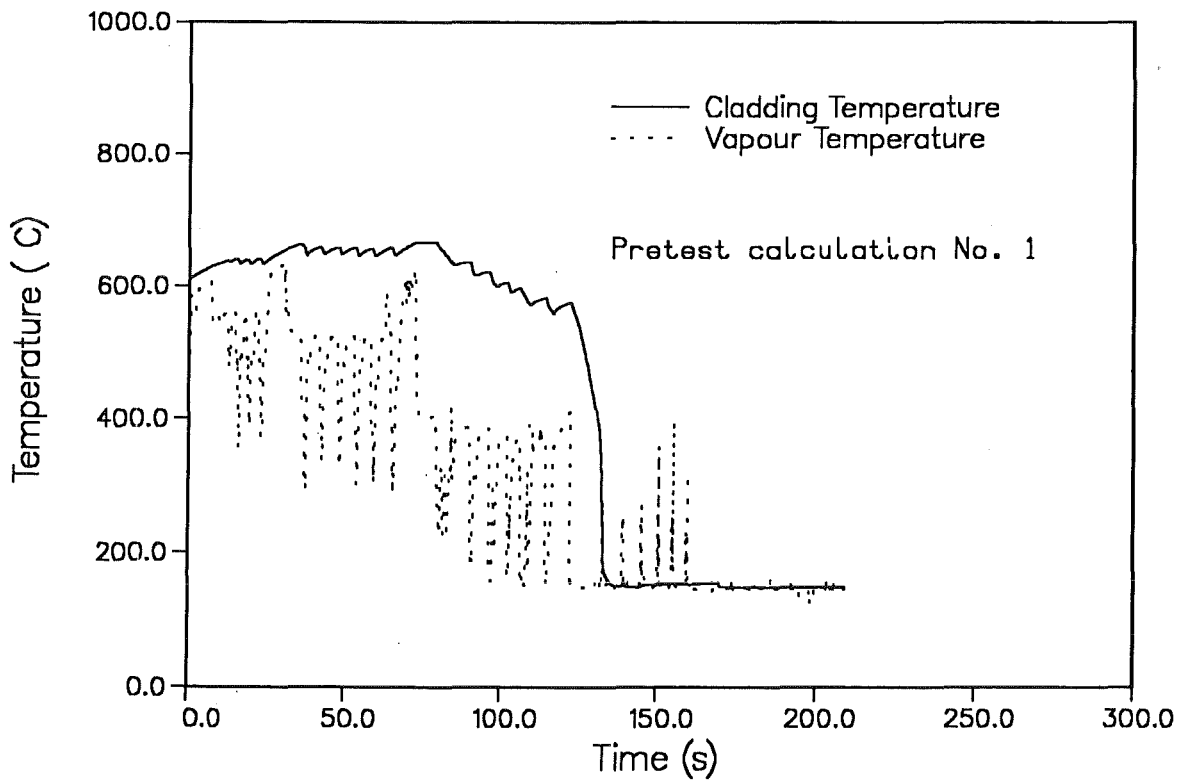
Figure 26. Test Nr. 8 - Cladding and vapour temperatures at level 4 (1).
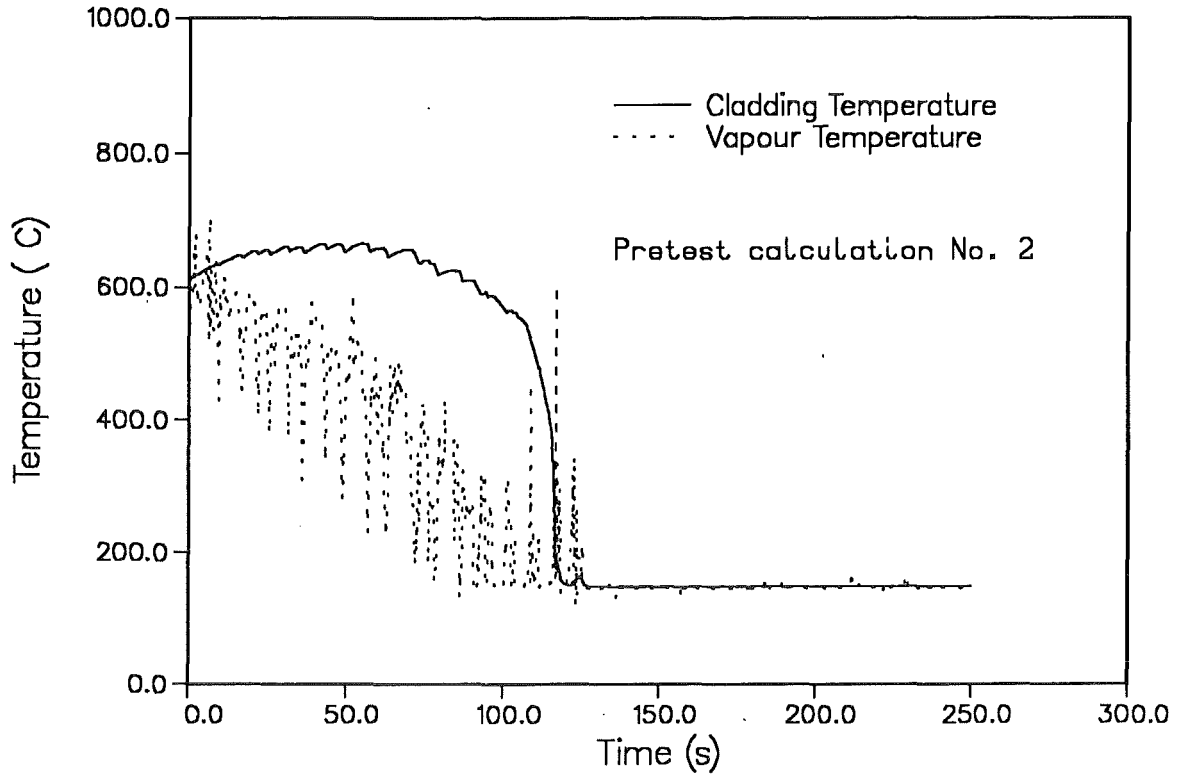
Figure 27. Test Nr. 8 - Cladding and vapour temperatures at level 4 (2).